Rock Mech. Rock Engng. (1996) 29 (1), 19–38

Rock Mechanics and Rock Engineering

Ground Response Curves for Rock Excavations Supported by Ungrouted Tensioned Rockbolts

By

V. Labiouse

Université Catholique de Louvain, Louvain-la-Neuve, Belgique

Summary

A numerical analysis has been developed for the design of ungrouted tensioned rockbolts as support of excavations under axisymmetric conditions. The bolts dimensions (length, cross-section, longitudinal and circumferential spacings), their stiffness, their pre-tension load and the delay of installation are taken into account. Moreover, the method effects three main improvements in the usual theory, taking into consideration: 1. the reaction force transferred to the rock mass in the bolts anchoring zone, 2. the elastic recompression of the carrying ring surrounding the excavation due to the bolts preload, and 3. the relative displacement of the bolts ends which has a repercussion on their tension.

Since the usual rock-support interaction analysis is only available when the rock mass and the support behave independently, an alternative solution has been explored for the bolting system (since it cannot be considered as an internal support). It consists to include the effect of the rockbolts into the ground reaction curve.

In this paper, the principles of the analysis are explained and a numerical application is taken.

1. Introduction

For a long time, bolting support is frequently used to stabilize underground excavations in rock masses. The determination of the rock reinforcement requirements has been commonly based on underground observations and on empirical approaches (rock mass classification systems). However, since a few years, this design procedure is completed by analytical and numerical evaluations. It enables a better qualitative and quantitative analysis of the rockbolts parameters.

Within the framework of this integral design method, this paper describes a numerical analysis to calculate ungrouted tensioned rockbolts supporting excavations under axisymmetric conditions.

After the presentation of the basic assumptions, the main improvements propounded in the developed approach are detailed, and the definition of a new ground reaction curve is introduced. Then, the principles of the analysis are

explained; and finally, a numerical application is taken to underline the differences between the developed method and the usual theory.

2. Basic Assumptions

The developed method is based on some fundamental assumptions:

2.1 Axisymmetry and Plane Strain Conditions

The problem is axisymmetric; it means that the analysis applies to a circular gallery of radius r_i driven in a homogeneous, isotropic rock mass subjected to a hydrostatic in situ stress field (magnitude p_0). It implies also to neglect the weight of the rock in the broken zone which develops around the excavation.

The length of the gallery is such that the problem is in a plane strain situation.

2.2 Model of Rock Mass Behaviour

The rock mass is assumed to have a perfect elastic-plastic behaviour and to be characterised by a Mohr-Coulomb's strength criterion:

$$\tau = c + \sigma \mathrm{tg}\varphi, \tag{1}$$

with τ the shear strength
σ the normal stress
φ the angle of friction
c the cohesion.

The idealized stress-strain relationships used in the analysis presented later are shown in Fig. 1. The rock is first assumed to be linearly elastic with Young's

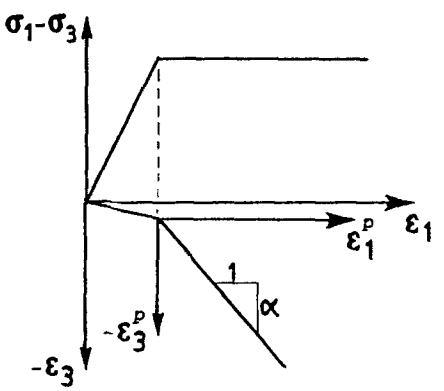

Fig. 1. Stress-strain relation of the rock mass

modulus E and Poisson's ratio ν. Then its behaviour becomes plastic and a non-associated flow rule is applied for the post-failure strains calculation:

$$\Delta\epsilon_3^p + \alpha\Delta\epsilon_1^p = 0 \tag{2}$$

with α the dilatancy parameter
$\Delta\epsilon_1^p$ and $\Delta\epsilon_3^p$ the increments of the major and minor principal strains (resp. the tangential ϵ_t and radial ϵ_r strains).

2.3 Bolting Support System

The ungrouted tensioned rockbolts are installed perpendicularly to the excavation surface, i.e. in radial directions (Fig. 2). Their characteristics are:

s_t : the circumferential spacing
s_l : the longitudinal spacing
L_b : the free length of the shank
A_b : the cross-sectional area of the shank
E_b : the Young's modulus of the bolting system, taking into account the deformation characteristics of the anchor, washer plate and bolt head. It can be measured from the load-extension curve determined by means of a pull-out test.
T_b : the tension load in the bolt
T_{b0}: the pre-tension load of the bolts
T_{bf}: the ultimate strength of the bolting system obtained from a pull-out test.

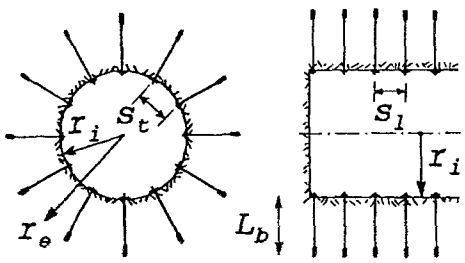

Fig. 2. Lie of the rockbolts

To keep the axisymmetry of the problem, it is assumed that the bolts spacings s_t and s_l are small enough to consider the gallery behaviour as uniform and independent of the location of a single bolt. Then, the support system provides an uniform radial pressure p_p which is related to the load T_b in the bolts by:

$$p_p = \frac{T_b}{s_l s_t}. \tag{3}$$

2.4 3D-Influence of the Working Face

The three-dimensional effect of the working face is considered introducing a fictitious pressure p_f on the inner face of the gallery (Panet, 1975; AFTES, 1986; Corbetta, 1990). This pressure depends on the unsupported span behind the excavation face. It allows to take into account the delay for support installation, with respect to the tunnelling process.

3. Main Improvements

The present approach effects three main improvements in the usual "convergence-confinement" analysis; it takes into consideration:

1. the reaction force transferred to the rock mass in the anchoring zone of the bolt,
2. the elastic recompression of the carrying ring surrounding the excavation, induced by the bolts preload,
3. the relative displacement of the bolts ends, and its repercussion on the tension in the rockbolts.

3.1 Reaction Force in the Anchoring Zone

Since the bolts have an unbonded length (Fig. 3), the load T_b in the shank is transferred without friction from the anchor head to the bond length (cement grout or resin). In consequence, the effect of these point anchored rockbolts must be simulated not only by an "action" pressure p_p applied on the surface (radius r_i), but also by a "reaction" pressure $p_p.r_i/r_e$ on the inner face of the anchoring zone (radius r_e). This influence is schematically represented in Fig. 4.

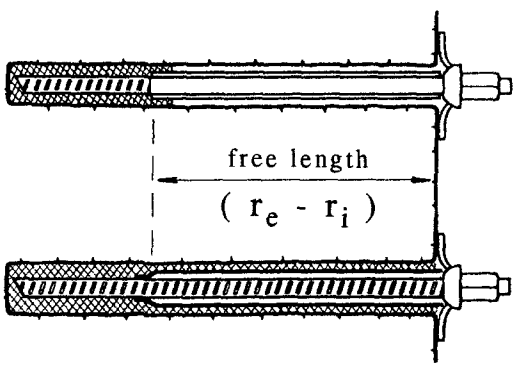

Fig. 3. Point anchored rockbolts

3.2 Elastic Recompression Due to the Pretension Load

In order to determine the stresses and displacements into the carrying ring ($r_i \leq r \leq r_e$) induced by the bolts preload T_{b0} (i.e. by the pressures $p_{p0} = T_{b0}/(s_l.s_t)$ and $p_{p0}.r_i/r_e$ applied at the inner and outer faces of the bolted ring), use is made of the Lamé's formulas (1852) (Appendix A):

$$\sigma_r = p_p \frac{r_i}{r_e + r_i}\left(1 + \frac{r_i r_e}{r^2}\right) \tag{4}$$

$$\sigma_t = p_p \frac{r_i}{r_e + r_i}\left(1 - \frac{r_i r_e}{r^2}\right) \tag{5}$$

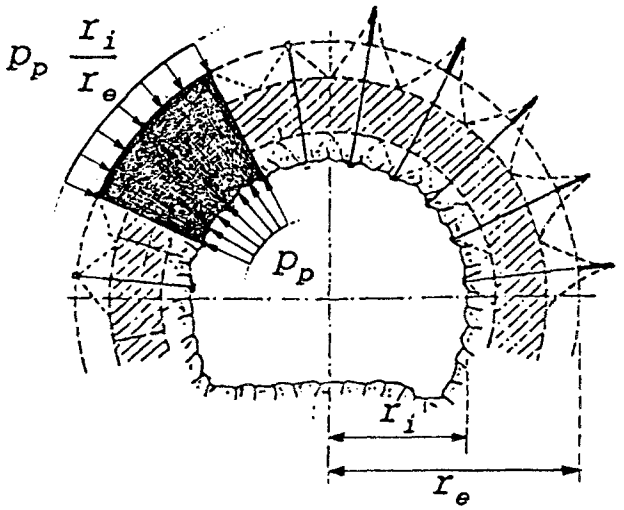

Fig. 4. Support pressure p_p and reaction pressure $p_p.r_i/r_e$ induced by the rockbolting system

$$u_r = \frac{1+\nu}{E} p_p \frac{r_i r}{r_e + r_i} \left(1 - 2\nu - \frac{r_i r_e}{r^2}\right). \tag{6}$$

These radial σ_r and tangential σ_t stresses due to the pretension load are represented in Fig. 5. It can be noted that the radial stress is bigger than the tangential one, and that the latter takes negative values (i.e. tension) between r_i and $\sqrt{r_i r_e}$.

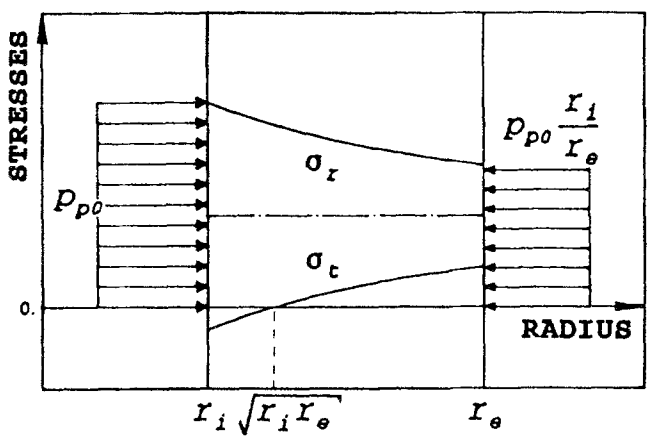

Fig. 5. Radial σ_r and tangential σ_t stresses due to the bolting pressures p_{p0} and $p_{p0}.r_i/r_e$

Now, this situation is just the opposite to the usual one encountered around underground excavations (where $\sigma_t > \sigma_r$ in both elastic and plastic zones); and consequently, the superposition of the preload to the initial situation before the bolts installation, will always be benefic, owing to the reduction of the difference between the major and minor principal stresses.

More particularly, if a part of the carrying ring was characterised by a plastic behaviour before the bolts installation, it will find temporarily an elastic behaviour again. Indeed, in a Mohr's circles plot (Fig. 6), the circles initially tangent to the Coulomb's straight line before the bolts preload, become then detached owing to the recompression of the carrying ring.

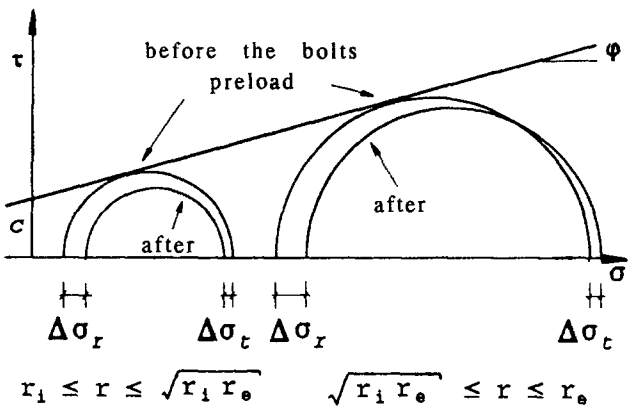

Fig. 6. Evolution of the Mohr's circles following the bolts preload

3.3 Tension Increase in the Rockbolts

After the support installation, the excavation restarts and the influence of the working face reduces progressively (this effect is simulated by a gradual decrease of the fictitious pressure applied on the gallery inner sides). The subsequent loosening of the rock mass induces an increase of the convergences. Figure 7 illustrates especially the relative displacement of the bolts ends and the elongation ΔL_b undergone by the shank:

$$\Delta L_b = (u_{ri} - u_{ri,pp0}) - (u_{re} - u_{re,pp0}), \tag{7}$$

with $u_{ri,pp0}$ and $u_{re,pp0}$ the displacements after the bolts preloading.

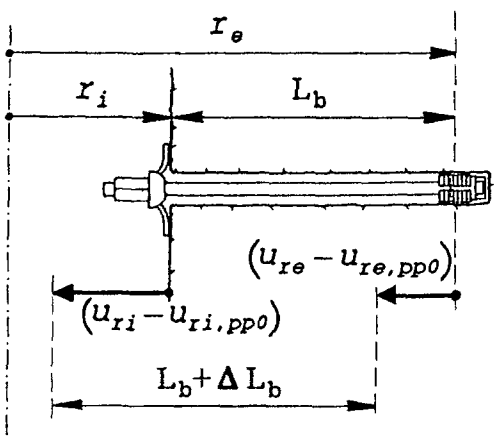

Fig. 7. Relative displacement of the bolts ends

This length variation ΔL_b has a repercussion on the tension T_b in the rockbolts:

$$T_b = T_{b0} + \Delta T_b = T_{b0} + \frac{\Delta L_b E_b A_b}{L_b}. \tag{8}$$

In consequence, the pressures p_p and $p_p.r_i/r_e$ generated at the inner and outer faces of the carrying ring, are the sum of two contributions:

$$p_p = p_{p0} + \Delta p_p = \frac{T_{b0} + \Delta T_b}{s_l s_t}. \tag{9}$$

4. Ground Reaction Curve of a Bolted Rock Mass

The rock-support interaction analysis requires the calculation of two variables: the radial wall convergence u_{ri} and the internal support pressure p_i. Usually, the equilibrium is found by the intersection of two characteristic lines in a (u_{ri}, p_i) diagram: the ground response curve C_v and the support reaction line C_f (Fig. 8). However, this kind of presentation is only available when the rock mass and the support behave independently; e.g. a concrete or shotcrete lining and steel arches.

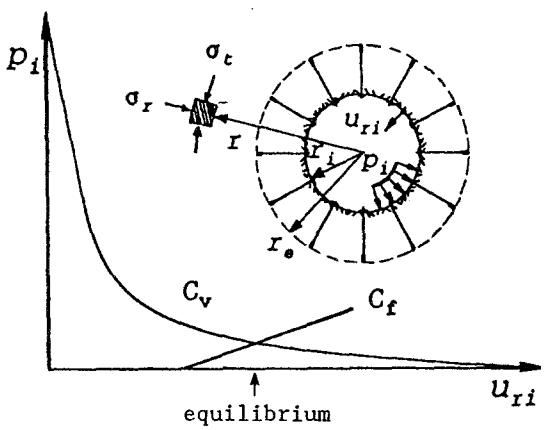

Fig. 8. Rock-support interaction: convergence curve C_v and confinement curve C_f

Now, as explained previously, the bolting system cannot be considered as an internal support since:

- the bolts transfer their reaction into the rock mass,
- their preload induces a recompression of the carrying ring,
- their elongation depends on the rock mass convergences and has a repercussion on their tension.

For these reasons, an alternative solution has been explored: it consists to include the effect of the ungrouted bolts into the ground reaction curve. Such a curve C_{vb} is shown in Fig. 9 near the characteristic line of an unsupported rock

mass C_v (usual presentation). A reaction line C_f for an internal support is also drawn. The equilibrium is reached when this line meets the curve of the bolts supported rock mass. Let's note that such a presentation has also been used by Stille et al. (1989) and Holmberg (1991) for grouted bolts.

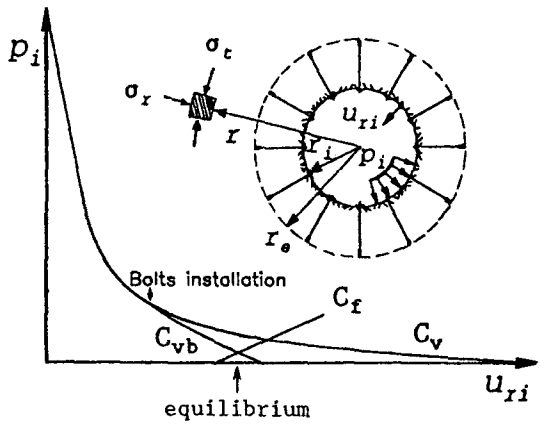

Fig. 9. Ground reaction curve C_{vb} for a rock mass supported with rockbolts

5. Principles of the Numerical Analysis

Within the specified assumptions, two calculation methods have been developed: an analytical one and a numerical one (Labiouse, 1993). Only the second approach will be presented hereafter.

Owing to the axial symmetry, the numerical analysis can be founded upon an one-dimensional model. Figure 10 illustrates the gridpoints (1) to (nbre) in the bolted zone ($r_i \leq r \leq r_e$), and (nbre + 1) to (nb) in the rock mass ($r \geq r_e$). Two nodes are used at the bolts anchoring point (radius r_e) in order to simulate the discontinuities induced by the reaction pressure $p_p.r_i/r_e$.

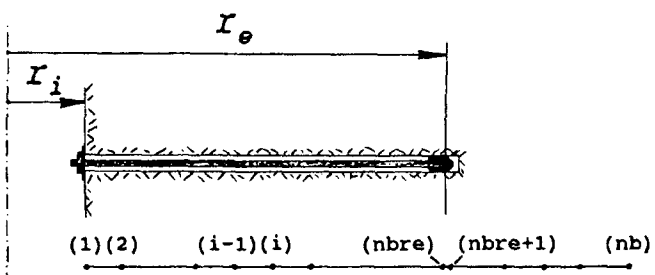

Fig. 10. One-dimensional model used for the numerical analysis

5.1 Calculation Procedure

Figure 11 presents a simplified "flow" diagram of the calculation procedure followed to take into account the three main improvements above-mentioned. The numbers between square brackets are explained hereafter in the text.

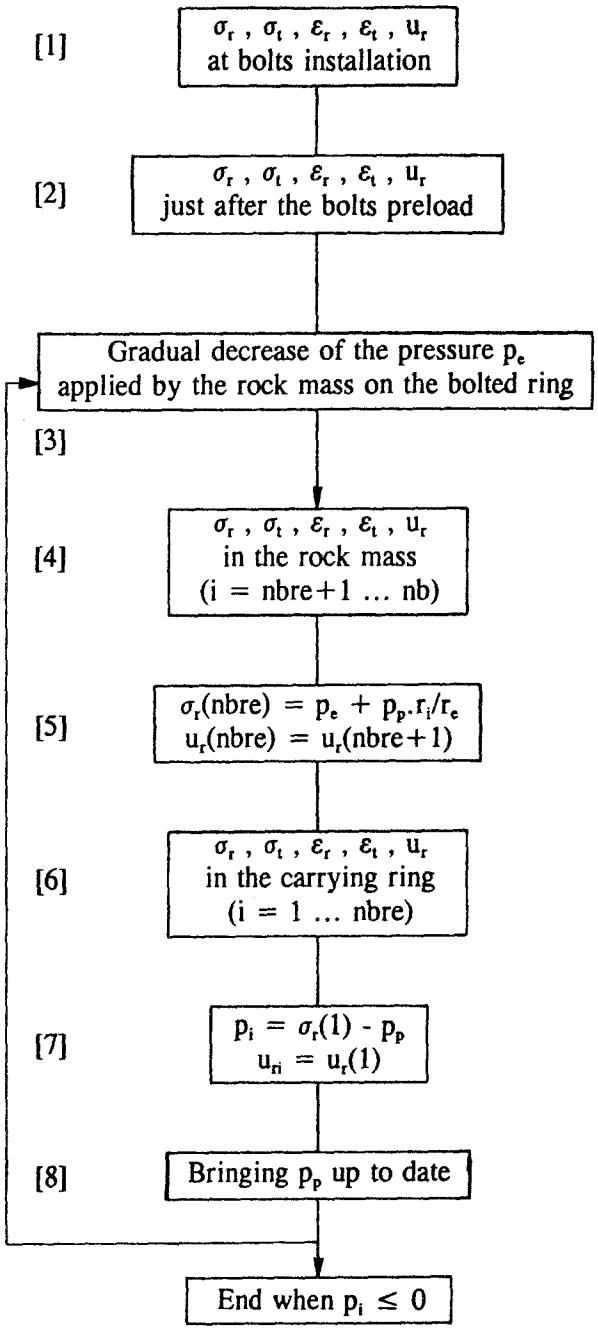

Fig. 11. Simplified "flow" diagram of the calculation procedure

At the initial situation (bolts installation, [1]), the stresses, strains and displacements around the excavation are evaluated using usual analytical formulas (Appendix B). Then, just after the bolts preload [2], the situation is obtained by adding to the previous one the elastic distributions induced by the pressures p_{p0} and $p_{p0}.r_i/r_e$ applied at the inner and outer faces of the reinforced zone (see Fig. 5).

Afterwards, the pressure applied by the rock mass on the carrying ring is gradually reduced [3]. The same analytical formulas as previously are used again to estimate the stresses, strains and displacements in the rock mass [4].

At the interface between the carrying ring and the rock mass [5], one can express the continuity of the displacement and the discontinuity of the radial stress (rise with a magnitude of $p_p.r_i/r_e$). From this, it is possible to calculate the tangential stress as well as the strains at gridpoint (nbre).

Then [6], the situation in the bolted zone is obtained numerically using a step by step procedure that successively determines the stresses, strains and displacement at the discretization points (from (nbre-1) to (1)). For this process, three behaviours need to be distinguished (Fig. 12): elastic, plastic and elasto-plastic. They will be treated succinctly in subheadings 5.2, 5.3 and 5.4.

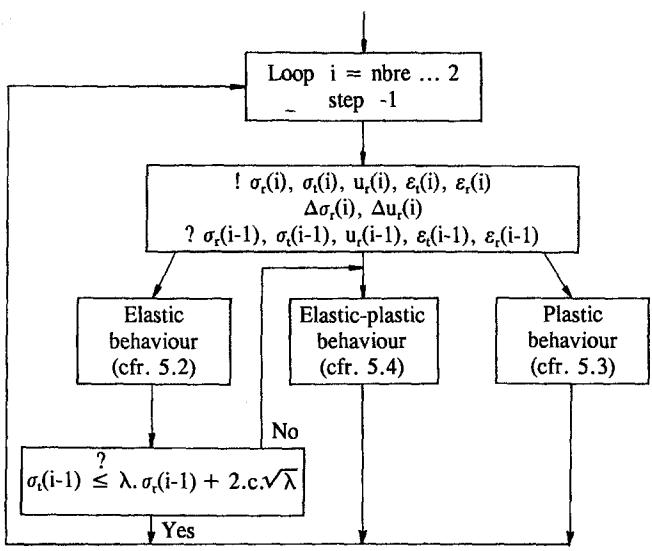

Fig. 12. Determination of the stresses, strains and displacements in the bolted ring

This step by step sequence of calculation is repeated several times till the unknown variables at node (1) are determined. So, can be calculated the convergence u_{ri} at the excavation surface and the associated internal pressure p_i [7]. On the other hand, since the bolts ends have a relative displacement $\Delta L_b = \Delta u_{ri} - \Delta u_{re} = \Delta u_r(1) - \Delta u_r(\text{nbre})$, their tension will increase and the pressure p_p generated by the bolting support need to be brought up to date [8].

These three latter variables u_{ri}, p_i and p_p are used to draw:

- in a (u_{ri}, p_i) diagram the ground reaction curve of the bolted rock mass,
- in a (u_{ri}, p_p) diagram the evolution of the tension in the rockbolts.

5.2 Elastic Behaviour

Let's first consider that the ring $(i-1)$ which lies between radii $r(i-1)$ and $r(i)$ has an elastic behaviour (Fig. 13). Using Lamé's formula (A-3) given in appendix A, the increment of displacement at node (i), i.e. $\Delta u_r(i)$, can be expressed as:

$$\Delta u_r(i) = \frac{(1+\nu)(1-2\nu)}{E[r^2(i) - r^2(i-1)]} r(i) \times \left[\Delta\sigma_r(i) \left(r^2(i) + \frac{r^2(i-1)}{(1-2\nu)} \right) - \Delta\sigma_r(i-1) r^2(i-1) \frac{2(1-\nu)}{(1-2\nu)} \right] \quad (10)$$

where $\Delta\sigma_r(i-1)$ and $\Delta\sigma_r(i)$ are the pressure variations on the inner and outer faces of the ring $[r(i-1), r(i)]$.

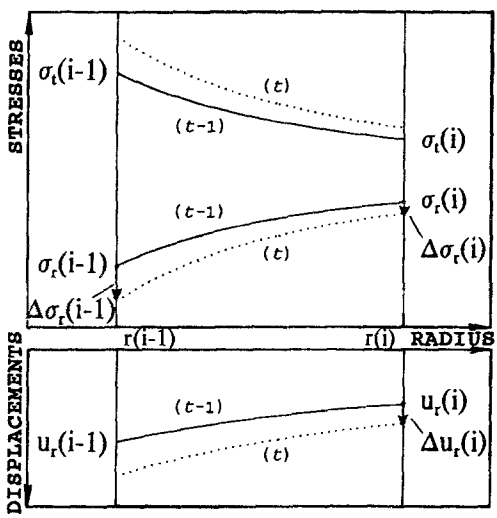

Fig. 13. Stresses and displacements when the ring $(r(i-1), r(i))$ has an elastic behaviour

Rewriting the above equation, one obtains:

$$\Delta\sigma_r(i-1) = \frac{1}{2(1-\nu)r^2(i-1)} \times \left[\Delta\sigma_r(i)[(1-2\nu)r^2(i) + r^2(i-1)] - \frac{\Delta u_r(i) E[r^2(i) - r^2(i-1)]}{(1+\nu)r(i)} \right]. \quad (11)$$

So, if the radial stress variation $\Delta\sigma_r(i)$ and the convergence increment $\Delta u_r(i)$ occuring at node (i) are known, an updated value of the stresses, strains and displacements at any point in the ring can be calculated using Lamé's formulas (A-1) to (A-5). More particularly, at gridpoint $(i-1)$:

$$\Delta\sigma_t(i-1) = \frac{1}{r^2(i) - r^2(i-1)}[2\Delta\sigma_r(i)r^2(i) - \Delta\sigma_r(i-1)[r^2(i) + r^2(i-1)]], \quad (12)$$

$$\Delta u_r(i-1) = \frac{(1+\nu)r(i-1)}{E[r^2(i) - r^2(i-1)]} \times [2(1-\nu)\Delta\sigma_r(i)r^2(i) - \Delta\sigma_r(i-1)[r^2(i) + (1-2\nu)r^2(i-1)]], \quad (13)$$

$$\Delta\epsilon_t(i-1) = \frac{(1+\nu)}{E[r^2(i) - r^2(i-1)]} \times [2(1-\nu)\Delta\sigma_r(i)r^2(i) - \Delta\sigma_r(i-1)[r^2(i) + (1-2\nu)r^2(i-1)]], \quad (14)$$

$$\Delta\epsilon_r(i-1) = \frac{(1+\nu)}{E[r^2(i) - r^2(i-1)]} \times [-2\nu\Delta\sigma_r(i)r^2(i) + \Delta\sigma_r(i-1)[r^2(i) - (1-2\nu)r^2(i-1)]]. \quad (15)$$

The elastic behaviour of the ring must then be verified with the condition:

$$\sigma_t(i-1) < \mathrm{tg}^2\left(\frac{\pi}{4} + \frac{\varphi}{2}\right)\sigma_r(i-1) + 2c\mathrm{tg}\left(\frac{\pi}{4} + \frac{\varphi}{2}\right). \quad (16)$$

If this inequality is not met, a plastic zone extends between the radii $r(i-1)$ and $r(i)$, and the ring needs to be treated pursuant to the procedure presented in subheading 5.4 (Fig. 12).

5.3 Plastic Behaviour

In this second case (Fig. 14), the stresses $\sigma_r(i-1)$ and $\sigma_t(i-1)$ are easily determined from the radial stress $\sigma_r(i)$ by the common relationships available for broken zones in axisymmetric problems (Appendix B):

$$\sigma_r(i-1) = (\sigma_r(i) + c\,\mathrm{cotg}\,\varphi)\left(\frac{r(i-1)}{r(i)}\right)^{(\lambda-1)} - c\,\mathrm{cotg}\,\varphi \quad (17)$$

$$\sigma_t(i-1) = \mathrm{tg}^2\left(\frac{\pi}{4} + \frac{\varphi}{2}\right)(\sigma_r(i) + c\,\mathrm{cotg}\,\varphi)\left(\frac{r(i-1)}{r(i)}\right)^{(\lambda-1)} - c\,\mathrm{cotg}\,\varphi. \quad (18)$$

Using the strains compatibility equation

$$\frac{d\epsilon_t}{dr} = \frac{\epsilon_r - \epsilon_t}{r} \quad (19)$$

the relations between strains and displacement

$$\epsilon_r = \frac{du_r}{dr} \quad \epsilon_t = \frac{u_r}{r} \quad (20)$$

and the non-associated flow rule (2), the strains and displacement at gridpoint $(i-1)$ can be evaluated from the strains at node (i):

$$u_r(i-1) = \epsilon_t(i) r(i-1) + \frac{\epsilon_t(i) - \epsilon_r(i)}{\alpha + 1} r(i-1) \left[\left(\frac{r(i)}{r(i-1)} \right)^{(\alpha+1)} - 1 \right], \quad (21)$$

$$\epsilon_t(i-1) = \epsilon_t(i) + \frac{\epsilon_t(i) - \epsilon_r(i)}{\alpha + 1} \left[\left(\frac{r(i)}{r(i-1)} \right)^{(\alpha+1)} - 1 \right], \quad (22)$$

$$\epsilon_r(i-1) = \epsilon_r(i) - \frac{\alpha}{\alpha + 1} (\epsilon_t(i) - \epsilon_r(i)) \left[\left(\frac{r(i)}{r(i-1)} \right)^{(\alpha+1)} - 1 \right]. \quad (23)$$

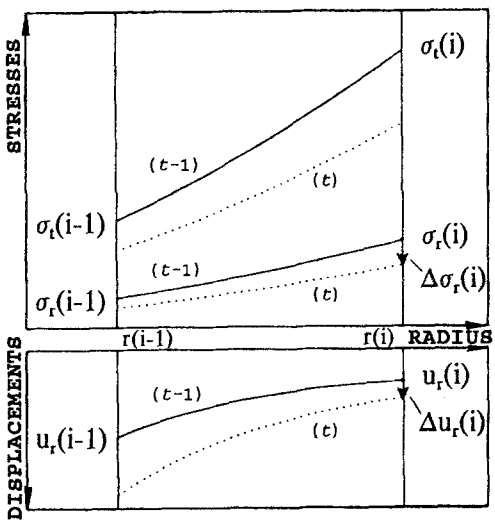

Fig. 14. Stresses and displacements when the ring $(r(i-1), r(i))$ has a plastic behaviour

5.4 Elastic-Plastic Behaviour

The analysis becomes a little more complicated due to the extension of the broken zone. The calculation is started from the latest known situation (at time $(t-1)$); at that moment, the ring is characterised by a plastic zone $[r(i-1), r_{ie}(t-1)]$ and an elastic zone $[r_{ie}(t-1), r(i)]$, as schematically represented by the solid lines in Fig. 15. Assuming that this latter zone keeps an elastic behaviour (dashed lines in Fig. 15), it is possible to calculate the stresses at $r_{ie}(t-1)$ from the radial stress variation $\Delta\sigma_r(i)$ and the convergence increment $\Delta u_r(i)$ occuring at node (i), using Eq. (11) and (12) where $r(i-1)$ is replaced by $r_{ie}(t-1)$.

Now, it stands to reason that the limit of the plastic zone will extend during the loosening of the rock mass. To appraise its enlargement, a shear yield function (corresponding to the Mohr-Coulomb's failure criterion) is used:

$$f = \sigma_t - \mathrm{tg}^2\left(\frac{\pi}{4} + \frac{\varphi}{2}\right)\sigma_r - 2c\,\mathrm{tg}\left(\frac{\pi}{4} + \frac{\varphi}{2}\right). \quad (24)$$

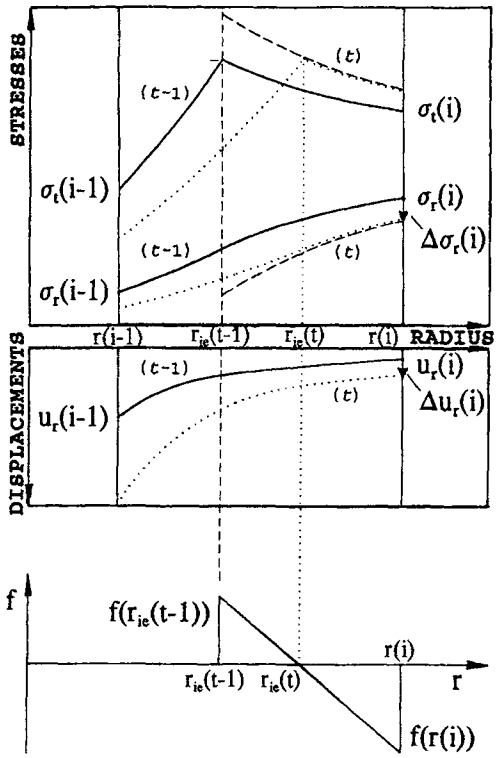

Fig. 15. Stresses and displacements when the ring $(r(i-1), r(i))$ has a partly elastic – partly plastic behaviour

Since radius $r_{ie}(t-1)$ is plasticized $(f(r_{ie}) > 0)$ and gridpoint (i) remains elastic $(f(r(i)) < 0)$, the point where the yield function meets the condition $f = 0$ can be found by interpolation (see lower part of Fig. 15). Once this new location of the plastic zone limit $r_{ie}(t)$ has been estimated, the stresses, strains and displacements in both elastic $[r_{ie}(t), r(i)]$ and plastic $[r(i-1), r_{ie}(t)]$ zones can be evaluated (dotted lines) using the relationships developed for the previous elastic and plastic behaviours.

6. Numerical Application

A 10 metres diameter gallery is driven at a depth of 400 metres (initial in situ stress $p_0 = 10000\,\text{kN/m}^2$) in a perfect elastic-plastic rock mass characterised by:

Young's modulus	$E = 10^6\,\text{kN/m}^2$
Poisson's ratio	$\nu = 0.30$
angle of friction	$\varphi = 34°$
cohesion	$c = 750\,\text{kN/m}^2$
dilatancy parameter	$\alpha = 1.2$

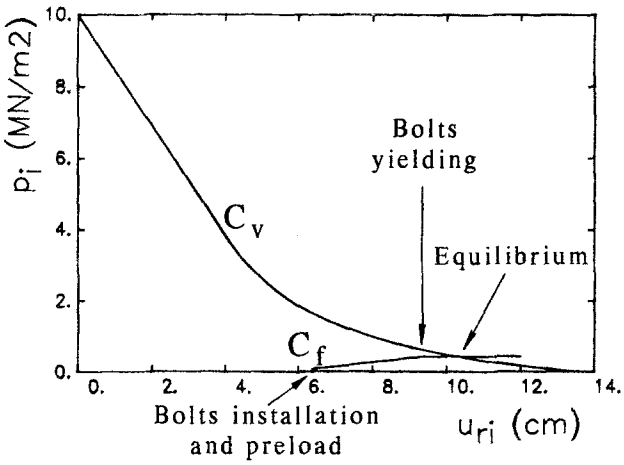

Fig. 16. Convergence and confinement curves according to the usual rock-support interaction analysis

The bolting support is installed one metre behind the working face (→ at that moment, the plastic zone has an extent of 1.2 m). Its specifications are:

Young's modulus	$E_b = 8\,10^7\,\text{kN/m}^2$
diameter	$\phi_b = 0.025\,\text{m}$
free length	$L_b = 6\,\text{m}$
bolts spacings	$s_l = s_t = 0.75\,\text{m}$
pre-tension load	$T_{b0} = 50\,\text{kN}$
yielding load	$T_{by} = 245\,\text{kN}$
ultimate failure load	$T_{bf} = 295\,\text{kN}$

Figure 16 shows the ground reaction curve C_v and the support reaction line C_f calculated according to the usual rock-support interaction analysis. Since the bolts reach their yielding load before the rock mass stabilization, it is obvious to determine the situation at equilibrium: $p_i = 436\,\text{kN/m}^2$ and $u_{ri} = 10.3\,\text{cm}$.

On the other hand, Fig. 17 represents the ground reaction curve C_{vb} for the rock mass supported with the ungrouted tensioned bolts, pursuant to the alternative solution presented at point 4. The evolution of the support pressure p_p is drawn in the lower (u_{ri}, p_p) diagram. For this second approach, the equilibrium is found for $p_i = 0\,\text{kN/m}^2$: $p_p = 386\,\text{kN/m}^2$ and $u_{ri} = 10.9\,\text{cm}$.

The stresses σ_r, σ_t and displacements u_r at equilibrium are represented in Fig. 18 for both methods: the usual one (dotted lines) and the new one (solid lines). Although there are few differences in the figure, the numerical results allow to establish that:

- the tension in the rockbolts calculated by the usual method (245 kN ≡ yielding load) is higher than our evaluation (217 kN). More particularly, it must be pointed out that the stiffness of the anchor bolt system is highly overestimated (75%!) by the usual approach;
- the convergences are larger in the new method.

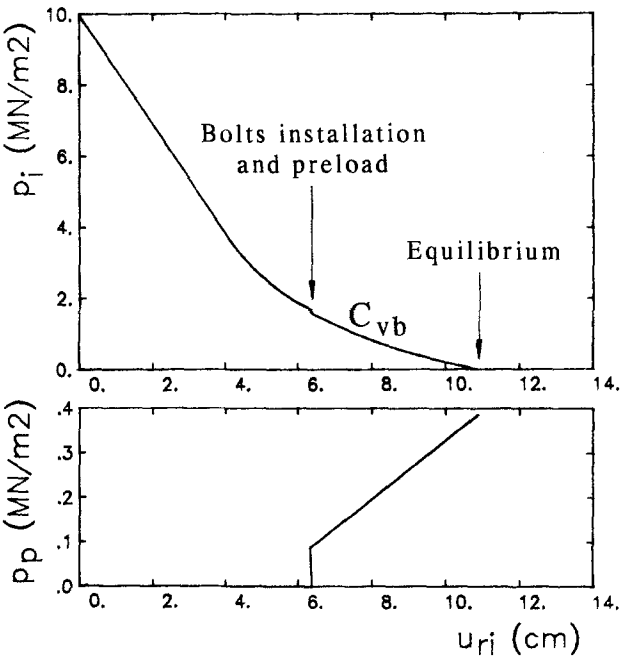

Fig. 17. Ground reaction curve for the rock mass supported with the ungrouted tensioned bolts; and evolution of the support pressure

These differences can easily be explained by the assumptions of the calculation methods:

- the usual theory assumes that the bolt anchoring point doesn't converge ($u_{re} = u_{re,pp0}$), and consequently, the shank elongation becomes equal to the increment of convergence at the gallery surface: $\Delta L_b = u_{ri} - u_{ri,pp0}$. On the other hand, the present approach takes into account the convergence of the anchoring point and the relative displacement of the bolts ends: $\Delta L_b = (u_{ri} - u_{ri,pp0}) - (u_{re} - u_{re,pp0})$.
- the usual method takes into consideration the action of the rockbolts on the excavations inner sides, but neglects the reaction force transferred to the rock mass in the anchoring zone. On the other hand, the new approach presents a comprehensive study.

These considerations emphasize that the stiffness of the bolting support evaluated by the new method is smaller than the one calculated by the usual theory.

7. Conclusion

The present paper has described a numerical analysis to calculate ungrouted tensioned rockbolts supporting excavations under axisymmetric conditions. The main improvements in the usual theory have been explained, and the differences

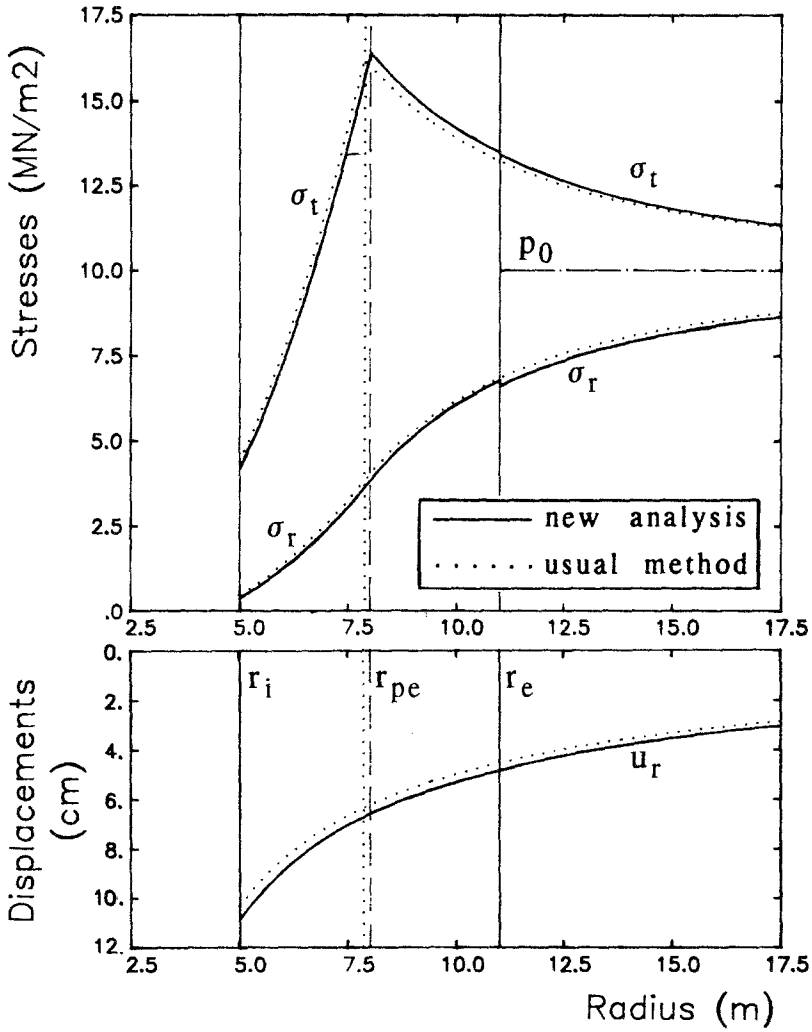

Fig. 18. Stresses and displacements at equilibrium

between both methods have been pointed out in a numerical application. In particular, it has been observed that a systematic bolting studied by the new approach is characterised by a much smaller stiffness than the one calculated by the usual method.

Finally, let's point out the very fast computation of the developed method. Indeed, half a minute is enough to obtain the ground reaction curve of a rock mass supported with a bolting support, and to calculate the distributions of the stresses, strains and displacements around the excavation. Consequently, such a method allows to perform quick parametrical studies; and so is helpful to understand the influence of the bolting characteristics (free length, delay of installation, pretension load, stiffness of the rockbolts) on the radial deformations and support stresses at equilibrium.

8. Appendix A

Lamé (1852) has determined the stresses, strains and displacements into hollow cylinders (inner and outer radii r_i and r_e, Young's modulus E, Poisson's ratio ν) induced by an internal pressure p_i and an external pressure p_e:

$$\sigma_r = \frac{1}{(r_e^2 - r_i^2)}\left[p_e r_e^2 - p_i r_i^2 - (p_e - p_i)\frac{r_e^2 r_i^2}{r^2}\right], \tag{A-1}$$

$$\sigma_t = \frac{1}{(r_e^2 - r_i^2)}\left[p_e r_e^2 - p_i r_i^2 + (p_e - p_i)\frac{r_e^2 r_i^2}{r^2}\right], \tag{A-2}$$

$$u_r = \frac{(1+\nu)(1-2\nu)}{E(r_e^2 - r_i^2)} r\left[p_e r_e^2 - p_i r_i^2 + (p_e - p_i)\frac{r_e^2 r_i^2}{(1-2\nu)r^2}\right], \tag{A-3}$$

$$\epsilon_t = \frac{(1+\nu)(1-2\nu)}{E(r_e^2 - r_i^2)}\left[p_e r_e^2 - p_i r_i^2 + (p_e - p_i)\frac{r_e^2 r_i^2}{(1-2\nu)r^2}\right], \tag{A-4}$$

$$\epsilon_r = \frac{(1+\nu)(1-2\nu)}{E(r_e^2 - r_i^2)}\left[p_e r_e^2 - p_i r_i^2 - (p_e - p_i)\frac{r_e^2 r_i^2}{(1-2\nu)r^2}\right]. \tag{A-5}$$

9. Appendix B

For the assumptions presented in the paper (excavation of radius r_i, initial in situ stress p_0, perfect elastic-plastic rock mass characterised by: Young's modulus E, Poisson's ratio ν, angle of friction φ, cohesion c, dilatancy parameter α), the "convergence-confinement" method gives an analytical solution.

The rock mass behaviour remains elastic as long as the internal pressure p_i acting on the gallery inner sides is higher than a limit:

$$p_{\text{lim}} = \frac{2(p_0 + c\operatorname{cotg}\varphi)}{(\lambda+1)} - c\operatorname{cotg}\varphi \tag{B-1}$$

with

$$\lambda = \operatorname{tg}^2\left(\frac{\pi}{4} + \frac{\varphi}{2}\right).$$

The stresses and displacement in this elastic medium are of the following forms:

$$\sigma_r = p_0 - (p_0 - p_i)\frac{r_i^2}{r^2}, \tag{B-2}$$

$$\sigma_t = p_0 + (p_0 - p_i)\frac{r_i^2}{r^2}, \tag{B-3}$$

$$u_r = \frac{(1+\nu)}{E}(p_0 - p_i)\frac{r_i^2}{r}. \tag{B-4}$$

When the internal pressure p_i becomes smaller than the limit pressure $p_{\lim}$, a broken zone appears and extends around the excavation. The limit of this plastic zone is given by:

$$r_{pe} = r_i \left[\frac{2(p_0 + c\,\mathrm{cotg}\,\varphi)}{(\lambda+1)(p_i + c\,\mathrm{cotg}\,\varphi)} \right]^{\left(\frac{1}{\lambda-1}\right)}. \tag{B-5}$$

The stresses and displacement take the following forms:

elastic zone ($r_{pe} \leq r \leq \infty$):

$$\sigma_r = p_0 - \frac{(\lambda-1)}{(\lambda+1)}(p_0 + c\,\mathrm{cotg}\,\varphi)\frac{r_{pe}^2}{r^2}, \tag{B-6}$$

$$\sigma_t = p_0 + \frac{(\lambda-1)}{(\lambda+1)}(p_0 + c\,\mathrm{cotg}\,\varphi)\frac{r_{pe}^2}{r^2}, \tag{B-7}$$

$$u_r = \frac{(1+\nu)}{E}\frac{(\lambda-1)}{(\lambda+1)}(p_0 + c\,\mathrm{cotg}\,\varphi)\frac{r_{pe}^2}{r}. \tag{B-8}$$

plastic zone ($r_i \leq r \leq r_{pe}$):

$$\sigma_r = (p_i + c\,\mathrm{cotg}\,\varphi)\left(\frac{r}{r_i}\right)^{(\lambda-1)} - c\,\mathrm{cotg}\,\varphi, \tag{B-9}$$

$$\sigma_t = \lambda(p_i + c\,\mathrm{cotg}\,\varphi)\left(\frac{r}{r_i}\right)^{(\lambda-1)} - c\,\mathrm{cotg}\,\varphi, \tag{B-10}$$

$$u_r = \frac{(1+\nu)}{E}\frac{(\lambda-1)}{(\lambda+1)}(p_0 + c\,\mathrm{cotg}\,\varphi)r\left[1 + \frac{2}{\alpha+1}\left(\left(\frac{r_{pe}}{r}\right)^{(\alpha+1)} - 1\right)\right]. \tag{B-11}$$

References

A.F.T.E.S. (1986): Recommendations for use of convergence – confinement method. Tunnels et Ouvrages Souterains 73 (1/2), 18.

Brown, E. T., Bray, J. W., Ladanyi, B., Hoek, E. (1983): Ground response curves for rock tunnels. J. Geotechn. Engng. 109 (1), 15.

Corbetta, F. (1990): Nouvelles méthodes d'étude des tunnels profonds. Calculs analytiques et numériques. Doctoral Thesis, Ecole National Supérieure des Mines de Paris.

Hoek, E., Brown, E. T. (1980): Underground excavations in Rock. The Institution of Mining and Metallurgy, London, 525 pp.

Holmberg, M. (1991): The mechanical behaviour of untensioned grouted rockbolts. Doctoral Thesis, Dept. of Soil and Rock Mechanics, Royal Institute of Technology, Stockholm.

Labiouse, V. (1993): Etudes analytique et numériques du boulonnage à ancrage ponctuel comme soutènement de tunnels profonds creusés dans la roche. Doctoral Thesis, Université Catholique de Louvain, Louvain-la-Neuve.

Lamé, G. (1852): Leçons sur la théorie de l'élasticité. Gauthiers-Villars, Paris.

Panet, M. (1975): Analyse de la stabilité d'un tunnel creusé dans un massif rocheux en tenant compte du comportement après la rupture. Rock Mech. Rock Engng. 8 (4).

Stille, H., Holmberg, M., Nord, G. (1989): Support of weak rock with grouted bolts and shotcrete. Int. J. Rock Mech. Min. Sci. 26 (1), 99.

Author's address: Dr. V. Labiouse, Université Catholique de Louvain, G. C., Unité Génie Civil, Bâtiment Vinci, B-1348 Louvain-la-Neuve, Belgium.